Turkish Journal of Electrical Engineering & Computer Sciences

http://journals.tubitak.gov.tr/elektrik/

Research Article

Turk J Elec Eng & Comp Sci
(2022) 30: 1115 – 1126

doi:10.3906/elk-2108-61

Biometric identification using panoramic dental radiographic images with few-shot learning

Musa ATAŞ[1,*], **Cüneyt ÖZDEMİR**[2], **İsa ATAŞ**[3], **Burak AK**[4], **Esma ÖZEROĞLU**[5]

[1]Computer Engineering, Engineering Faculty, Siirt University, Siirt, Turkey
[2]Computer Technology Department, Vocational School of Technical Sciences, Siirt University, Siirt, Turkey
[3]Computer Technology Department, Diyarbakır Vocational School of Technical Sciences, Dicle University, Diyarbakır, Turkey
[4]Periodontology Department, Dentistry Faculty, Mersin University, Mersin, Turkey
[5]Büyükçekmece Oral and Dental Health Center, İstanbul, Turkey

Received: 09.08.2021 • **Accepted/Published Online:** 14.12.2021 • **Final Version:** 21.03.2022

Abstract: Determining identity is a crucial task especially in the cases of mass disasters such as tsunamis, earthquakes, fires, epidemics, and in forensics. Although there are various studies in the literature on biometric identification from radiographic dental images, more research is still required. In this study, a panoramic dental radiographic (PDR) image-based human identification system was developed using a customized deep convolutional neural network model in a few-shot learning scheme. The proposed model (PDR-net) was trained on 600 PDR images obtained from a total of 300 patients. As the PDR images of the patients were very different in terms of pose and intensity, they were first cropped by the domain experts according to the region of interest and adjusted to standard view with histogram equalization. A customized data augmentation approach was applied in order for the model to generalize better while it was being trained. The proposed model achieved a prediction accuracy of 84.72% and 97.91% in Rank-1 and Rank-10, respectively, by testing 144 PDR images of 72 patients that had not been previously used in training. It was concluded that well known similarity metrics such as Euclidean, Manhattan, Cosine, Pearson, Kendall's Tau and sum of absolute difference can be utilized in few-shot learning. Moreover, Cosine and Pearson similarity achieved the highest Rank 1 score of 84.72%. It was observed that as the number of rank increased, the Spearman and Kendall's Tau metrics had the same success as Cosine and Pearson. Based on the superimposed heatmap image analysis, it was determined that the maxillary, mandibular, nasal fossa, sinus and other bone forms in the mouth contributed biometric identification. It was also found that customized data augmentation parameters contributed positively to biometric identification.

Key words: Deep learning, few-shot learning, forensic informatics, human identification, panoramic dental radiographs

1. Introduction

Dental records are effectively used by forensic experts to identify deceased individuals. [1–3] studies in the literature have shown that teeth can be preserved extremely well in harsh environmental conditions, especially under high temperature, humidity and pressure, and contain significant information regarding personal identification. Moreover, the 2014 INTERPOL Disaster Victim Definition Guide emphasized that a number of methods included in forensic odontology are the primary and most reliable identification tools [1]. In addition,

*Correspondence: hakmesyo@gmail.com

[1]INTERPOL Disaster Victim Identification Guide (2014). [online]. Website https://www.interpol.int/content/download/589/file/18Y1344%20E%20DVI_Guide.pdf [accessed .25.10.2021]

Petju et al. reported that after the Indian Ocean tsunami disaster in Thailand dental records contributed significantly (46.2%) in the identification of the victims [4]. While the periapical radiographs concentrate on the image of a few teeth in a local area in the mouth, panoramic imaging mostly focuses on all teeth, including the entire oral cavity, maxilla and mandible [5]. In this study, focus was placed on panoramic dental images, which are supposed to positively contribute to biometric identification and offer a holistic approach. There exist many full or semi automatic machine learning studies based on the alignment and characteristics of the teeth, mouth internal structure and dental morphology known as automatic dental identification system (ADIS) [6–10]. Alternatively, manual approaches can also be used to analyze dental images. When using such approaches, the specialist should have sufficient knowledge on tooth morphology, dental restorations, periodontal tissue features, pathology and other anatomical features. However, manual approaches require a considerable amount of time and effort and are also error prone [11, 12]. In addition, the relatively few images of a patient, long time between the captured images, various X-Ray devices used, pose angle, exposure time, different contrast and brightness values further complicate identification from panoramic dental radiographic (PDR) images. In one of the first studies conducted on human identification from PDR images, Ajaz and Kathirvelu achieved 90% accuracy on 30 test data [13]. They followed an image processing based methodology and matched dental works such as crowns, fillings and bridges, in the PDR images. However, they did not test it on nondental works datasets. The first studies in this field were mostly conducted according to model-based methods using tooth segmentation and digital image processing techniques, and focused only on teeth. The major weakness of such methods was their fragility due to their algorithmic and rule-based nature. On the other hand, according to [14, 15], the maxillary, mandibular, nasal fossa, sinus and other inter mouth bones also contribute to identification. In recent studies [15–18], deep learning and, in particular, convolutional neural network (CNN) architecture have been adopted in the classification of medical images. Gurses and Oktay [16] used the Mask R-CNN and SURF methods for matching dental images. They achieved 80.39% accuracy with the tooth-wised approach for Rank-1. Similarly, Oktay [5] achieved 81% identification success in Rank-1 by adopting the fusion of support vector machine (SVM), probabilistic graphical model and single shot multibox detector (SSD) techniques. In these studies [5, 16], the authors applied the SURF method to the tooth images determined by Mask CNN instead of directly applying the SURF method to the PDR images. The disadvantage of this approach is that it does not benefit from intraoral structures. In addition, changes that may occur on individual teeth, such as tooth loss or an operation, may adversely affect the result. Lai et al. [11] developed a learnable connected attention network for biometric identification based on deep CNN and utilized the cosine similarity distance metric. Authors claimed that, the channel attention module contributes to more precise recognition results. The advantages of the proposed cosine loss method over the categorical cross entropy approach were tried to be shown in the study, but no study was conducted on the effects of this method on other datasets and frequently used CNN models. Consequently, they achieved accuracies of 87.21% and 95.34% for Rank-1 and Rank-5, respectively. Fan et al. [15] developed a customized Dent-net CNN model and obtained accuracies of 85.16% for Rank-1 and 97.74% for Rank-5 by using the cosine similarity. Working with a large number of PDR images and performing tests is an advantage in the related study, but the positive effect of the ring based data augmentation method on the results has not been examined adequately. Moreover, ring/patch based approach may lead to significant information loss.

The difference between previous studies and ours is that they only used cosine similarity as a measure of similarity. In this study, the effects of Pearson, Spearman, Kendall's Tau, Eucledian, Manhattan and sum of absolute difference similarity metrics were investigated along with Cosine similarity. In addition, the

contributions of other structures in the mouth were ignored because previous studies generally focused only on the teeth. Almost all of the biometric identification studies based on PDR images in the literature were developed using the few-shot learning methodology. This is because in biometric identification, contrary to the well-known CNN based classification problems, the number of classes is quite high and few images are available for each class. However, in normal classification problems, each class has a large number of images, such as in well known MNIST database. Thus, the number of images in each class and number of classes change inversely in the few-shot learning and CNN based schema. Another major difference between the two is related with the learning strategy. In classic classification approaches, in general, sparse categorical cross entropy is used as a loss function, while softmax activation is used as an activation function. However, in few-shot learning, embedded layers in the fully connected network are used to calculate the similarity distances between the images at hand to all remaining in the dataset. Thus, few-shot learning can be regarded as a lazy learner like K-NN [19, 20].

The main purpose of our article is to develop a deep learning model to identify the patient from pdr images using few shot learning technique. Overall, this study provides two contributions to the current literature: 1) It determined that the Kendall's Tau, Spearman and Pearson correlation coefficients explained in detail in Section 2.4.2 can be used as alternatives to the Cosine similarity measure, which has generally been utilized in previous studies and 2) it showed that the patch approach suggested in [16], and [12] did not improve the performance of the model as expected. Moreover, it was determined that well-known data augmentation technique can yield more successful results for biometric identification using PDR images.

The paper is structured as follows: the preprocessing, real-time data augmentation, PDR-net model generation, training and inference strategies are explained in the materials and methods section. Then, experimental results section is presented. Finally, the concluding remarks and future perspectives are given.

2. Materials and methods

2.1. PDR image dataset

The PDR images of 372 patients treated between 2018 and 2020 in Mersin University Faculty of Dentistry Periodontology clinics were acquired. Each patient had at least two PDR images taken at different times. A total of 144 images of 72 patients, approximately one-quarter of the image dataset of the 372 patients, were randomly separated as the test dataset, which was completely isolated and never seen by the proposed PDR-net during the training process. Six hundred images of the remaining 300 individuals were used in the training of the PDR-net model. Images were taken with a Planmeca Promax 2D digital panoramic x-ray device (anodic voltage 50-84 KV, current 0,5-16 mA, Planmeca, Finland), which was available in the clinic. As the PDR images were taken at different dates and different exposure times and angles, the images of the patients may not be exactly similar and/or registered. This was one of the factors that complicated the identification. The rows in Figure 1 present the PDR images of the different patients taken at different times. In Figure-1, the first line shows the PDR images of the same patient, with the difference in intensity, and subsequent operations on the teeth. In the image on the right of the second line, there is an overexposure problem and the resulting loss of information. In the bottom line, we encounter the blurring problem.

2.2. Preprocessing

As the raw PDR images were not completely of the same standard content, the most appropriate region, in other words, the area containing the most information, in the image was marked and cropped. This meant that images with an average resolution of 1680x1100 were reduced to a resolution of approximately 1250x700 pixels.

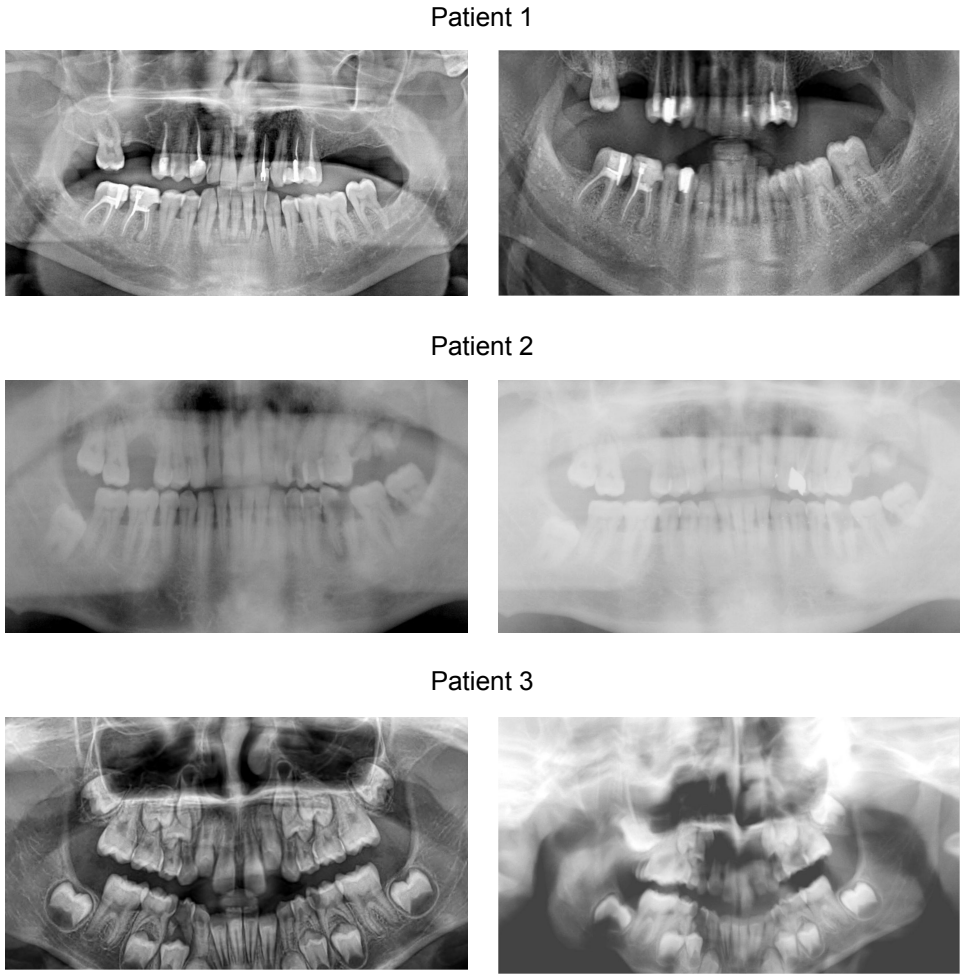

Figure 1. PDR images of patients.

Afterwards, the preprocessing algorithm resized all the images from different resolutions to 1100x500 standard pixel resolution. Next, the darkness and lightness of the images were adjusted to a similar contrast range by using the histogram equalization method. Histogram equalization is an fundemental image processing technique that adjusts the global contrast of the image based on the pixel density distribution of the image histogram. The main purpose of using this technique is to transform low-contrast images into relatively higher-contrast images. Finally, the images were resized to 120x264 pixel resolution along with keeping aspect ratio of the original PDR image in order to feed the proposed PDR-net. Figure 2 depicts the whole preprocessing stages.

2.3. Data augmentation

It is well known that CNN based deep learning models require the existence of a large database of images for each class to be identified. However, in few-shot learning, as the name implies, each class has a limited number of images. Such as in the case of this study, each patient had only two PDR images. What complicated the problem further was that even these two images of the same patient can be different from each other in terms of exposure time, angle and zoom ratios. In order to overcome data scarcity, data augmentation was

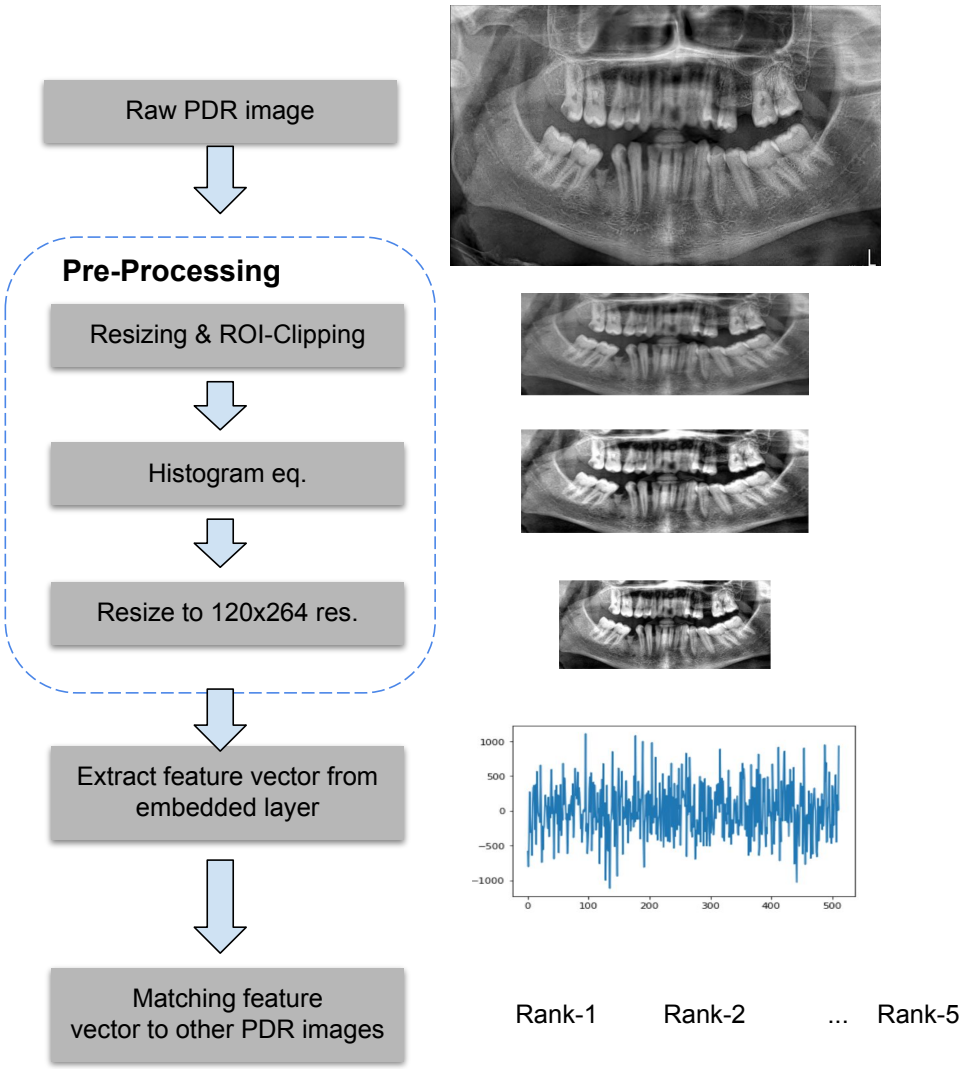

Figure 2. Overview of the PDR-net architecture.

considered as a possible solution. The previous study [15] utilized data augmentation by taking patches and using them as white circular masks in random places in the image and achieved improved performance. The methodology proposed by [15] was implemented in the present study, however, the results were not promising. Nevertheless, it was believed that data augmentation would improve the results as proposed by [15]. Thus, to improve the generalization capability of the proposed model, data augmentation was carried out by using ImageDataGenerator available in the Keras library in each iteration. The model was fine-tuned while it was being trained using the on flow property of the Keras library. Table 1 summarizes the optimized parameters and their corresponding values of the ImageDataGenerator obtained after numerous trials. The rotation range refers to how many degrees the image will be rotated relative to the center. The problem may occur due to the patient's head turning while the PDR image is being taken. It is observed that rotation happens in a range of 3° in general. Similarly, it is considered reasonable to enlarge or reduce PDR images within 0.1 zoom range and 0.05 width shift and height shift range. In addition, it was estimated from the change in the PDR images

that the brightness range could be in the range of 0.7-1.1 and the rescale value could be 1/255. While choosing these values, our general approach started from extreme values and continued in the form of reduction until PDR images were formed that were acceptable and similar to the images in the dataset.

Table 1. Fine-tuned parameters of data augmentation.

Parameter	**Value**
rotation_range	3
width_shift_range	0.05
height_shift_range	0.05
zoom_range	0.1
brightness_range	[0.7, 1.1]
rescale	1./255

2.4. PDR-net

The CNN-based deep learning model proposed in this study, namely PDR-net, consisted of two phases: the training phase and the inference phase.

2.4.1. Training phase

As shown in Table 2 and Figure 3, the PDR-net model was comprised of both CNN layers and fully connected neural network blocks. First, the PDR images were resampled into images with a resolution of 120x264 pixels after the preprocessing stage. As the PDR images were gray-scaled, the number of channels in the CNN input layer was fixed to one. The CNN block was composed of three convolution layers. Although increasing the number of layers in the model improves the performance, this should be well justified as it also increases computational complexity [21]. Thus, in the PDR-net model, number of layers was fixed to three.

Table 2. PDR-net architecture.

Layer (type)	**Patch size:Stride**	**Output shape**	**Param#**
input	-	120 x 264 x 1	-
convolution	3 x 3 : 1	120 x 264 x 64	640
max pool	2 x 2 : 2	60 x 132 x 64	0
convolution	3 x 3 : 1	60 x 132 x 128	73,856
max pool	2 x 2 : 2	30 x 66 x 128	0
convolution	3 x 3 : 1	30 x 66 x 256	295,168
max pool	2 x 2 : 2	15 x 33 x 256	0
flatten	-	126,720	0
feature map 1:linear	-	1024	129,762,304
droput:50%	-	1024	0
feature map 2:linear	-	512	524,800
droput:50%	-	512	0
feature map 3:linear	-	256	131,328
droput:50%	-	256	0
dense:linear	-	(302) number of patients	77,614
Total Params:	-	-	130,865,710

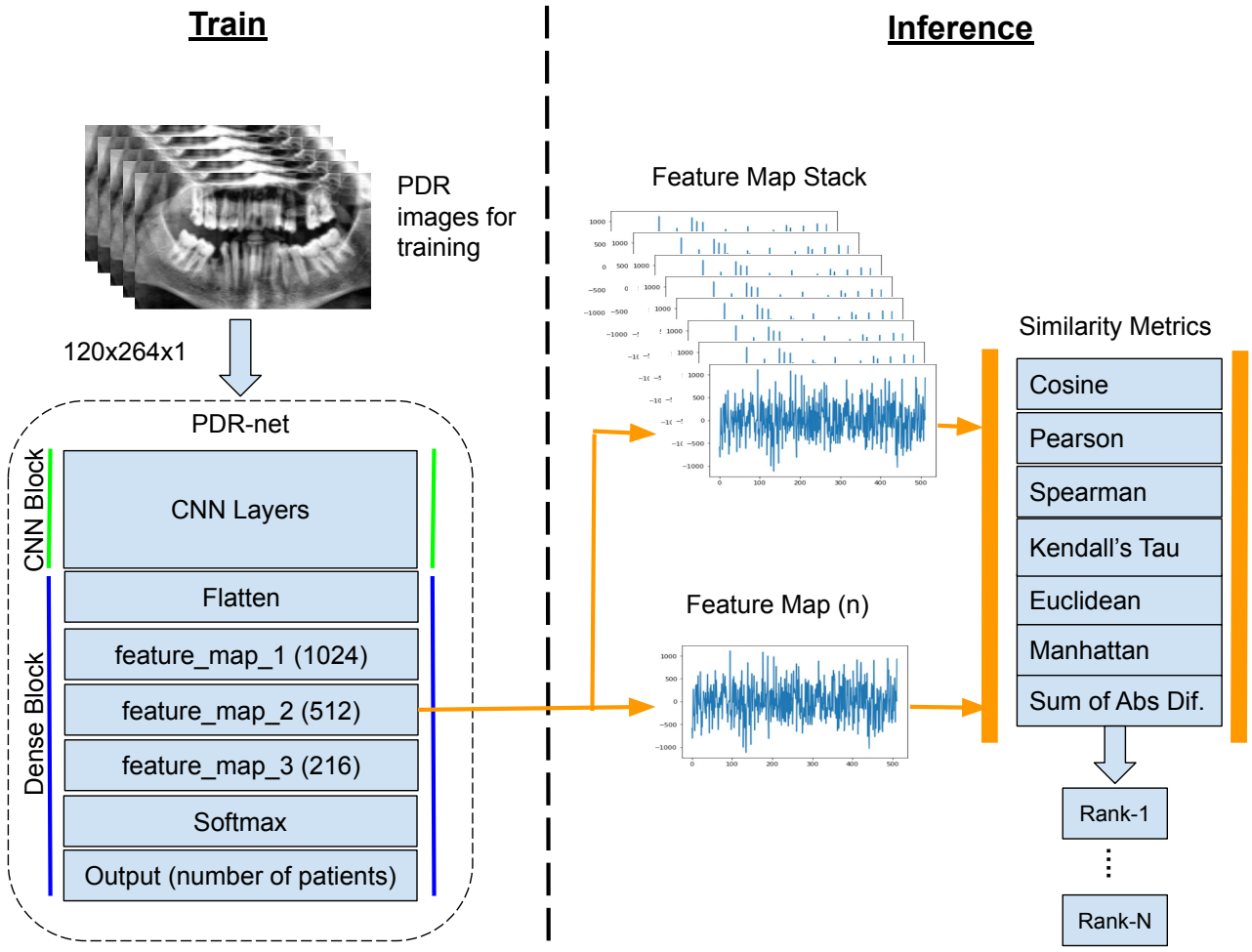

Figure 3. Visualization of the proposed PDR-net model (train and inference phases).

In all of the layers, a parametric rectified linear unit (PRELU) [22] and a maxpool with a 2 by 2 patch and a stride 2 value were utilized as the activation function and pooling strategy, respectively. In the first CNN layer, in order to extract the necessary features from the raw PDR image, 64 pieces of 3 by 3 filters were convoluted. Then, the convolution process was performed on 128 and 256 pieces with 3 by 3 filters. The flattening layer connected the last pooling layer of the CNN block to the dense block by transforming it into a one-dimensional array. The fully connected neural network (dense) block consisted of three hidden dense layers. Each layer is actually a kind of representation or embedding layer with higher abstraction capacity [23]. In the first layer of the block, 126,720 input neurons were compressed to 1024, aiming to encode information in a lower dimensional space. Similarly, feature map 2 and feature map 3 encoded the streaming information to 512 and 256 sizes, respectively. The "categorical cross entropy" loss function and softmax activation function were used to assign the output layer to the patient class labels.

The PDR-net model was developed using the Tensorflow and Keras frameworks. A server with Intel Pentium i7, K80 Nvidia GPU and 16GB Ram hardware was used for the training and testing of the model. Learning was carried out at 48,000 iterations with a batch size of 32 and with an initial learning coefficient

of 0.001. In order to minimize divergence problems in learning, the factor and patience parameters of the ReduceLROnPlateau object in the Keras library were assigned values of 0.8 and 15, respectively. With these values, the learning rate was multiplied by 0.8 when necessary, ensuring smooth learning.

2.4.2. Inference phase

In few-shot learning, inference is achieved by the comparison of the embedding layer in the dense block of the model. In this context, the Cosine, Euclidean, Manhattan, Pearson, Spearman, Kendall's Tau and sum of absolute difference (SAD) distance methods were used. The Cosine similarity metric, which has also been used in previous studies [15], produces a value in the range of [-1, 1]. The similarity decreases as the value gets closer to -1. Similarly, Pearson, Spearman and Kendall's Tau correlation coefficient values are also in the range of [-1, 1]. However, unlike the Cosine similarity, the value of 0 represents the least similarity. The Euclidean and Manhattan metrics measure the distances of two vectors in spatial space within the interval [0, INF]. SAD is an approach that measures primitive distance by taking the absolute difference of the vectors and summing them up. In this respect, a value of 0 indicates maximum similarity in the Euclidean, Manhattan, and SAD metrics.

The biggest advantage of the few-shot learning approach when compared to the traditional classification is that it is not required to prevent overfitting of the model during the training stage. Furthermore, few-shot operates on classes (not cases) has never seen before. Moreover, once few-shot learning has been trained, it can successfully classify even the classes that were previously not included in the training set and encountered for the first time in the testing phase, using the similarity criterion. Experiments have usually shown that the middle layer is the most effective embedding layer in the generalization capacity of the model. The embedding layer in the PDR-net model, actually corresponds to the feature_map_2 seen in Figure 3.

3. Experimental results

In this study, 600 PDR images of 300 patients and 144 PDR images of 72 patients were used for training and testing purposes, respectively. Test and train sets are randomly divided into %80 and %20. As neither the code nor the data sets of biometric identification studies available in the literature are accessible, it is impossible to make a completely fair and rational comparison between those and the present study. In order to overcome this, the model developed in the study presented in [15] was reimplemented and its performance was tested using the PDR dataset. As shown in Figure 3, in the performance evaluation of the PDR-net model, the second embedding layer with 512 nodes was used in the inference (test) phase as it gave better results during the training phase.

The main distinction between the training and inference phases of the present study was that the training was achieved as a normal classifier, while in the inference phase, the similarities were compared using the few-shot learning approach. To achieve this, the query image was compared one by one with all the images present in the dataset, excluding the query image itself.

In the PDR-net model, the average time for a prediction was approximately 0.02 s. This represents the time required for the prediction of feature map 2. On the other hand, it took approximately 0.24 ms to measure the similarity distance of the two feature maps. That is to say, the prediction was approximately 100 times slower than the similarity calculation. As each query took a considerably longer time, a different approach was adopted for working with real-time applications and large-scale datasets. In this approach, initially the prediction of all PDR images was recorded in an array. Thus, the fast access to the element of the array increased the speed of the overall identification process.

The grad-cam method proposed in [24] was used to determine the regions to focus on in terms of identification while the PDR-net performed its predictions. In order to achieve this, the matrix composed by the filters in the last CNN layer of the proposed PDR-net model was superimposed on the real PDR image (Figure 4). The first column in Figure 4 shows the CNN feature map indicating the regions that were focused on. The first row of Figure 4 indicates an unmatched case (low similarity score) where regions that were focused on (shown with yellowish to reddish colors) were very few. However, the second row of Figure 4 shows a matched case (high similarity score) and the superimposed map in this row indicates the regions that were focused on with brighter yellowish to reddish colors spread over a wider area, covering the maxillary, mandibular, nasal fossa, sinus and other bone forms in the mouth.

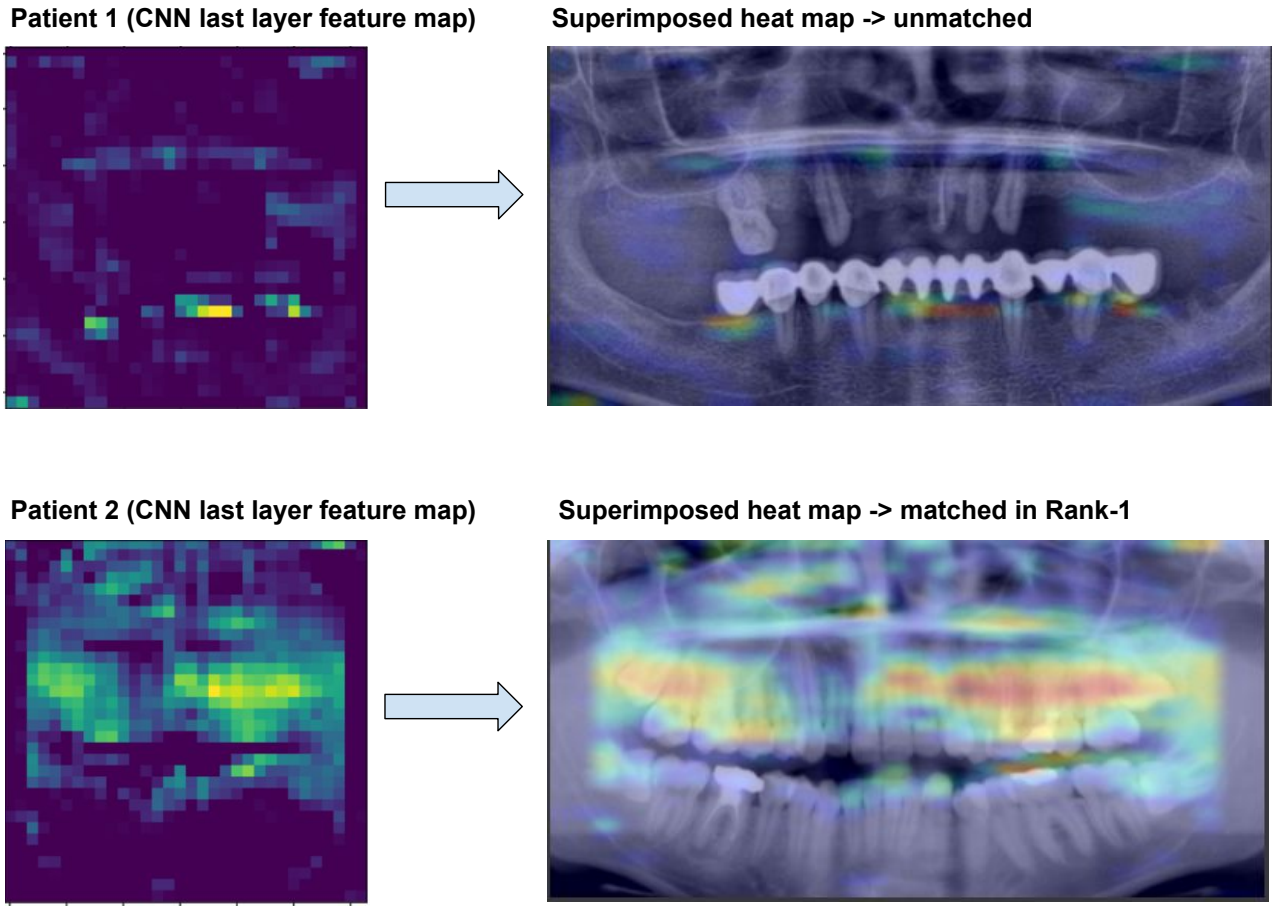

Figure 4. Visualization of the superimposed feature map onto PDR test image for both matched and unmatched cases.

In the study, the Rank-N method enumerated from Rank-1 to Rank-10 was used to evaluate the accuracy of the proposed model. The Rank-1 value is a performance criterion that is measured when the queried image has the highest similarity with other images of the same patient. Likewise, Rank-N can be expressed as the implementation of the aforementioned method on the first N elements.

In this study, the customized deep learning model was compared with the models (EfficientNet) previously trained in other datasets (Imagenet) using transfer learning. However, as the results were much lower than expected, it was decided to work on customized deep learning models. Rank-1 to Rank-5 achievements reported

in previous studies [5, 13, 15] were summarized and compared with the PDR-net model suggested in this study (Table 3).

The values in the first three rows of Table 3 were obtained from the datasets of the respective authors. However, as a result of applying the method used by Fei [15] to the dataset of the present study, it was observed that the success rates decreased for almost all ranks.

Table 4 summarizes the similarity criteria results used in the study and shows that the Cosine, Pearson, Spearman and Kendall's Tau metrics exhibited similar success values. If only Rank 1 is taken into consideration it can be seen that with a success rate of 84.72%, Cosine similarity and Pearson correlation surpass the others. However, as the Rank increased the Cosine, Pearson Spearman and Kendall's Tau methods produced similar results and reached an accuracy rate of 97.91% in Rank-10. The Euclidean, Manhattan and SAD methods achieved lower success rates in almost all Ranks.

Table 3. Detailed comparisons of studies in the field of human identification in terms of Rank-N percentage accuracy.

Studies	**Rank-1**	**Rank-2**	**Rank-3**	**Rank-4**	**Rank-5**	**Rank-10**
Ajaz & Kathirvelu (own dataset) [13]	43.25%	NA	NA	NA	48.47%	NA
Oktay (own dataset) [5]	68.42%	NA	NA	NA	76.07%	NA
Fei [15] (own dataset)	85.16%	NA	NA	NA	97.74%	NA
Proposed PDR-net (our dataset)	84.72%	90.27%	91.66%	93.05%	95.14%	97.91%
Fei [15] (our dataset)	66.80%	70.98%	75.83%	80.00%	82.77%	91.80%

Table 4. Performance comparisons of similarity distance metrics vs Rank-N.

Similarity Distance	**Rank-1**	**Rank-2**	**Rank-3**	**Rank-4**	**Rank-5**	**Rank-10**
Cosine similarity	**84.72%**	**87.50%**	**90.27%**	**94.44%**	**96.52%**	**97.91%**
Pearson correlation	**84.72%**	**87.50%**	**90.27%**	**94.44%**	**96.52%**	**97.91%**
Spearman correlation	82.63%	86.80%	**90.27%**	93.05%	94.44%	**97.91%**
Kendall's Tau correlation	82.63%	86.11%	**90.27%**	93.75%	94.44%	**97.91%**
Euclidean distance	75.00%	79.16%	82.63%	84.02%	85.41%	89.58%
Manhattan distance	73.61%	79.16%	81.94%	84.02%	85.41%	88.19%
Sum of absolute difference	73.61%	79.16%	81.94%	84.72%	85.41%	88.19%

4. Conclusion

Biometric identification, based on PDR images is extremely important for forensic informatics. In this study, a customized deep learning model known as PDR-net was developed based on few-shot learning. Unlike previous studies, the effectiveness of the Pearson, Spearman, Kendall's Tau, Euclidean, Manhattan and SAD metrics along with Cosine similarity distance were investigated in this study. In addition, it is found that the random position mask (white ring) and the patches taken from six different places suggested in [16] had a limited contribution to the identification process on the PDR image dataset of the study. On the contrary, during the training phase, data augmentation with the proposed parameters yielded more successful results. The experimental results revealed that Cosine and Pearson similarity criterion outperformed the other metrics with a success rate of 84.72% in terms of Rank-1. The superimposed heatmap image of the attention regions on the real image, visualized in the last layer of the CNN block, provided an insight to judge whether the model made rational decisions or not. Based on the heatmap images, it was confirmed that the maxillary, mandibular,

nasal fossa, sinus and other bone forms in the mouth contributed positively to biometric identification as stated in previous studies [14, 15]. The trained PDR-net model detected test images with the reported success rates without being retrained through few-shot learning.

In further studies, the effectiveness of Siamese network and contrastive, triplet and cross entropy loss functions developed for this model will be considered. Furthermore, as mentioned in [25], 1-D LBP encoding can be used to abstract the representation of the last layer in the CNN block and the embedded layers in the Dense block and use this as a feature map.

References

[1] Fereira JL, Fereira AE, Ortega AI. Methods for the analysis of hard dental tissues exposed to high temperature. Forensic Science International 2008; 178 (2): 119-124. doi: 10.1016/j.forsciint.2007.12.009

[2] Holden JL, Clement JG, Phakey PP. Age and temperature related changes to the ultrastructure and composition of human bone mineral. Journal of Bone and Mineral Research 1995; 10 (9): 1400-1409. doi: 10.1002/jbmr.5650100918

[3] Beale DR. The importance of dental records for identification. New Zealand Dental Journal 1991; 87 (389): 84–87. doi: 10.5455/aim.2015.23.49-52

[4] Petju M, Suteerayongprasert A, Thongpud R, Hassiri K. Importance of dental records for victim identification following the Indian ocean tsunami disaster in Thailand. Public Health 2007; 121 (4): 251–257. doi: 10.1016/j.puhe.2006.12.003

[5] Oktay AB. Human identification with dental panoramic radiographic images. IET Biometrics 2018; 7 (4): 349–355, doi:10.1049/iet-bmt.2017.0078

[6] Abdel-Mottaleb M, Nomir O, Nassar DE, Fahmy G, Ammar HH. Challenges of developing an automated dental identification system. In: IEEE 46th Midwest Symp. on Circuits and Systems Conference; Cairo, EGYPT;2003. pp. 411–414.

[7] Jain AK, Chen H. Matching of dental X-ray images for human identification. Pattern Recognition 2004; 37 (7): 1519–1532. doi:10.1016/j.patcog.2003.12.016

[8] Nassar DEM, Ammar HH. A neural network system for matching dental radiographs. Pattern Recognition 2007; 40 (1): 65–79. doi:10.1016/j.patcog.2006.04.046

[9] Zhou J, Abdel Mottaleb M. A content-based system for human identification based on bitewing dental X-ray images. Pattern Recognition 2005; 38 (11): 2132–2142. doi:10.1016/j.patcog.2005.01.011

[10] Heinrich A, Güttler FV, Schenkl S, Wagner R, Teichgräber UKM. Automatic human identification based on dental X-ray radiographs using computer vision. Scientific reports 2020; 10 (1): 1-13. doi:10.1038/s41598-020-60817-6

[11] Lai Y, Fan F, Wu Q, Ke W, Liao P et al. LCANet: Learnable Connected Attention Network for Human Identification Using Dental Images. IEEE Transactions on Medical Imaging 2021; 40 (2): 905-915. doi: 10.1109/TMI.2020.3041452

[12] Chen H, Jain, AK. Tooth contour extraction for matching dental radiographs. In: 17th International Conference on Pattern Recognition; Cambridge, UK;2004. pp. 522–525.

[13] Ajaz A, Kathirvelu D. Dental biometrics: computer aided human identification system using the dental panoramic radiographs. In: 2013 international conference on communication and signal processing; Melmaruvathur, INDIA;2013, pp. 717–721.

[14] Gorza L, Mânica S. Accuracy of dental identification of individuals with unrestored permanent teeth by visual comparison with radiographs of mixed dentition. Forensic Science International 2018; 289 (1):337–343. doi:10.1016/j.forsciint.2018.06.004

[15] Fan F, Ke W, Wu W, Tian X, Lyu T et al. Automatic human identification from panoramic dental radiographs using the convolutional neural network. Forensic Science International 2020; 314 (1): 121,130. doi: 10.1016/j.forsciint.2020.110416

[16] Gurses A, Ayse BO. Human Identification with Panoramic Dental Images using Mask R-CNN and SURF. In: 5th International Conference on Computer Science and Engineering UBMK; Diyarbakır, TURKEY; 2020 pp.232-237.

[17] Lee JH, Kim DH, Jeong SN, Choi SH. Detection and diagnosis of dental caries using a deep learning-based convolutional neural network algorithm. Jornal of Dentistry 2018; 77: 106-111. doi: 10.1016/j.jdent.2018.07.015

[18] Suzuki K. Overview of deep learning in medical imaging. Radiological physics and technology 2017; 10 (3): 257-273. doi:10.1007/s12194-017-0406-5

[19] Liu B, Yu X, Yu A, Zhang P, Wan G et al. Deep few-shot learning for hyperspectral image classification. IEEE Transactions on Geoscience and Remote Sensing 2018; 57 (4): 2290-2304. doi: 10.1109/TGRS.2018.2872830

[20] Wang Y, Yao Q, Kwok JT, Ni LM. Generalizing from a few examples: A survey on few-shot learning. ACM Computing Surveys 2020; 53 (3): 1-34. doi:10.1145/3386252

[21] Ataş M, Yardimci Y, Temizel A. A new approach to aflatoxin detection in chili pepper by machine vision. Computers and electronics in agriculture 2010; 87: 129-141. doi: 10.1016/j.compag.2012.06.001

[22] He K, Zhang X, Ren S, Sun J. Delving deep into rectifiers: Surpassing human-level performance on imagenet classification. In: IEEE international conference on computer vision; Santiago, CHILE; 2015 pp.1026-1034.

[23] Nonis F, Barbiero P, Cirrincione G, Olivetti EC, Marcolin F et al. Understanding Abstraction in Deep CNN: An Application on Facial Emotion Recognition. Progresses in Artificial Intelligence and Neural Systems. SINGAPORE: Springer, 2021, pp. 281-290.

[24] Selvaraju RR, Cogswell M, Das A, Vedantam R, Parikh D et al. Grad-CAM: visual explanations from deep networks via gradient-based localization. In: IEEE International Conference on Computer Vision; Venice, ITALY; 2017; pp:618–626.

[25] Ataş M. Hand tremor based biometric recognition using leap motion device. IEEE Access 2017; 5: 23320-23326. doi: 10.1109/ACCESS.2017.2764471